Title

A novel chromosome segregation mechanism during female meiosis.

Journal

Molecular biology of the cell, 27(16)

ISSN

1059-1524

Authors

McNally, Karen Perry
Panzica, Michelle T
Kim, Taekyung
et al.

Publication Date

2016-08-01

DOI

10.1091/mbc.e16-05-0331

Peer reviewed

A novel chromosome segregation mechanism during female meiosis

Karen Perry McNally[a], Michelle T. Panzica[a], Taekyung Kim[b,c], Daniel B. Cortes[a], and Francis J. McNally[a,*]

[a]Department of Molecular and Cellular Biology, University of California, Davis, Davis, CA 95616; [b]Ludwig Institute for Cancer Research, San Diego, CA 92093; [c]Department of Cellular and Molecular Medicine, University of California, San Diego, La Jolla, CA 92093

ABSTRACT **In a wide range of eukaryotes, chromosome segregation occurs through anaphase A, in which chromosomes move toward stationary spindle poles, anaphase B, in which chromosomes move at the same velocity as outwardly moving spindle poles, or both. In contrast, *Caenorhabditis elegans* female meiotic spindles initially shorten in the pole-to-pole axis such that spindle poles contact the outer kinetochore before the start of anaphase chromosome separation. Once the spindle pole-to-kinetochore contact has been made, the homologues of a 4-µm-long bivalent begin to separate. The spindle shortens an additional 0.5 µm until the chromosomes are embedded in the spindle poles. Chromosomes then separate at the same velocity as the spindle poles in an anaphase B–like movement. We conclude that the majority of meiotic chromosome movement is caused by shortening of the spindle to bring poles in contact with the chromosomes, followed by separation of chromosome-bound poles by outward sliding.**

Monitoring Editor
Kerry S. Bloom
University of North Carolina

Received: May 26, 2016
Revised: Jun 13, 2016
Accepted: Jun 14, 2016

INTRODUCTION

Eukaryotic chromosome segregation occurs in two mechanistically distinct phases termed anaphase A and anaphase B. During anaphase A, chromosomes typically move toward stationary spindle poles; during anaphase B, chromosomes maintain a constant distance from the poles as the poles separate (Inoué and Ritter, 1978). In this article, we describe an unconventional variation of anaphase A in which spindle poles move inward toward stationary chromosomes. Conventional anaphase A is driven by the shortening of microtubule bundles that have plus ends terminating at kinetochores and minus ends terminating at the spindle pole (Rath and Sharp, 2011). Attachment of chromosomes to the depolymerizing plus ends is mediated by the microtubule-binding components of the outer kinetochore, the NDC80 complex and Kinetochore Null (KNL-1; Cheeseman *et al.*, 2006). Anaphase B is driven, in some species, by the outward sliding of antiparallel interpolar microtubules by the bipolar kinesin 5 (Straight *et al.*, 1998; Brust-Mascher *et al.*, 2009). During the first mitosis of the *Caenorhabditis elegans* zygote, anaphase B is instead driven by cortical dynein, which pulls on astral microtubules extending outward from the spindle poles (Saunders *et al.*, 2007). Chromosomes maintain a constant distance from the separating spindle poles, and kinetochores are required to keep the chromosomes attached to the separating poles (Oegema *et al.*, 2001). *C. elegans* chromosomes are holocentric, and kinetochores extend down their entire length (Albertson and Thomson, 1982; Moore *et al.*, 1999); however, microtubule plus ends still terminate at kinetochores (Howe *et al.*, 2001; O'Toole *et al.*, 2003). Thus end-on attachments are required for both anaphase B and anaphase A. In addition to the mechanical requirement for these attachments, end-on attachments at kinetochores are believed to be essential for the recognition of bipolar attachment of replicated sister chromatids in mitosis and homologous chromosomes during meiosis I (Nasmyth, 2002).

Some features of *C. elegans* female meiotic spindles suggest that different mechanisms might be involved in chromosome segregation. First, *C. elegans* female meiotic spindles are acentriolar

This article was published online ahead of print in MBoC in Press (http://www.molbiolcell.org/cgi/doi/10.1091/mbc.E16-05-0331) on June 22, 2016.

*Address correspondence to: Francis J. McNally (fjmcnally@ucdavis.edu).

Abbreviations used: APC, anaphase-promoting complex; ASPM, abnormal spindle, microcephaly; BMK, bimC-like kinesin; DHC, dynein heavy chain; GFP, green fluorescent protein; KLP, kinesin-like protein; KNL, kinetochore null; RZZ, rod zw10 zwilch; ZWL, zwilch; ZYG, zygote defective.

(Albertson and Thomson, 1993). However, unlike acentriolar female meiotic spindles of the mouse, which concentrate the core pericentriolar proteins γ-tubulin and pericentrin at their poles (Gueth-Hallonet *et al.*, 1993; Carabatsos *et al.*, 2000), *C. elegans* female meiotic spindle poles lack the pericentriolar proteins γ-tubulin (McNally *et al.*, 2006), SPD-2/CEP192 (Kemp *et al.*, 2004), and SPD-5 (Hamill *et al.*, 2002; McNally *et al.*, 2012). Instead, MEI-1/katanin (McNally *et al.*, 2006), LIN-5/NuMA, and Abnormal Spindle and Microcephaly 1 like (ASPM-1; Ellefson and McNally, 2011) are concentrated at discrete spindle poles throughout *C. elegans* meiosis, and katanin is required to target ASPM-1 and organize microtubule minus ends into these discrete poles (McNally and McNally, 2011). Second, conserved kinetochore proteins are assembled into extremely large, cup-shaped structures that cap each end of either a meiosis I bivalent or a meiosis II sister chromatid pair (Howe *et al.*, 2001; Monen *et al.*, 2005; Dumont *et al.*, 2010). This structure is likely an adaptation necessitated by the holocentric nature of *C. elegans* kinetochores, as holocentry does not allow for the conventional two-step loss of cohesion during meiosis, and other holocentric organisms have adopted unusual meiotic chromosome structures (Heckmann *et al.*, 2014). KNL-1 is required for mitotic anaphase (Desai *et al.*, 2003) and the assembly of outer kinetochore proteins into meiotic cup-shaped kinetochores, yet depletion of KNL-1 does not affect the overall velocity of meiotic anaphase chromosome separation (Dumont *et al.*, 2010). In addition, kinetochore microtubules with plus ends terminating at the cup-shaped kinetochores have not been observed during *C. elegans* female meiosis; instead, the most prominent microtubule structures are bundles that extend from pole to pole, making only lateral contacts with chromosomes (Howe *et al.*, 2001; Wignall and Villeneuve, 2009; Muscat *et al.*, 2015). Thus chromosomes are located in microtubule-poor channels.

Dumont *et al.* (2010) proposed that, during *C. elegans* meiosis, microtubule polymerization between separating homologues generates an outward pushing force on chromosomes. Three observations supported this model. First, no tubulin was observed outside of separating chromosomes, suggesting that there are no spindle poles during anaphase. Second, the microtubule-poor channels observed during metaphase filled with microtubules during anaphase. Third, the microtubule dynamics regulator CLS-2 was observed between homologues at metaphase and was required for anaphase chromosome separation (Dumont *et al.*, 2010). This proposed molecular mechanism is analogous to the mechanism segregating replicated copies of the R1 plasmid by parM polymerization (Salje *et al.*, 2010).

Muscat *et al.* (2015) proposed an alternate model in which cytoplasmic dynein on meiotic chromosome surfaces transports chromosomes through the microtubule-poor channels by motoring toward the minus ends of the interpolar bundles. Three observations supported this model. First, microtubule-poor channels were observed during normal bipolar anaphase by single-time-point imaging. Second, cytoplasmic dynein was found associated with the cup-shaped kinetochores of monopolar, prometaphase spindles and on the outward face of anaphase chromosomes on bipolar spindles. Third, inhibition of cytoplasmic dynein resulted in lagging chromosomes during anaphase (Muscat *et al.*, 2015). This proposed molecular mechanism is analogous to the transport of membrane vesicles on microtubules.

Another unusual feature of *C. elegans* female meiotic spindles is that after activation of the anaphase-promoting complex (APC) but before initiation of chromosome segregation, spindles shorten dramatically in the pole-to-pole axis and then elongate again during chromosome separation (Yang *et al.*, 2003). The purpose of APC-dependent spindle shortening has been unclear, as it has not been observed during mitotic anaphase in either *C. elegans* or other commonly studied organisms. Here we use quantitative time-lapse imaging to test specific aspects of the Dumont and Muscat models. We find that chromosomes are indeed located in microtubule-poor channels throughout anaphase. However, because bivalents are larger than previously assumed, we find that they move only a fraction of their own length within the channels. Instead, we find that spindle shortening substitutes for conventional anaphase A by moving poles inward to overlap with the chromosomes before loss of cohesion. We also find that dynein dissociates from chromosomes before anaphase onset and that the microtubule dynamics regulator, ZYG-8, is required for anaphase B.

RESULTS

Chromosomes are located between interpolar microtubule bundles during wild-type, bipolar anaphase but move less than a chromosome diameter through the microtubule-poor channels

To test whether separating chromosomes travel through microtubule-poor channels as proposed by Muscat *et al.* (2015) or whether microtubule bundles extend between separating chromosome pairs as proposed by Dumont *et al.* (2010), we analyzed time-lapse sequences of meiotic embryos in utero within worms expressing green fluorescent protein (GFP):tubulin and mCherry::histone. Under optimal imaging conditions, chromosomes were observed exclusively between interpolar microtubule bundles when the chromosomes began separating (Figure 1A; 13/16 time-lapse sequences). One of the features required for optimal imaging is that the spindle remains perfectly parallel to the plane of focus. In the example shown in Figure 1A, four microtubule bundles and three separating pairs of homologous chromosomes remained in focus for nearly all of anaphase I. Between 0 and +90 s, chromosomes clearly separated by 0.83 µm within microtubule-poor channels. This early movement involves a decrease in distance between the chromosome and apparent end of the spindle and is thus analogous to anaphase A. All subsequent chromosome separation (1.5 µm) between +90 and +210 s was accompanied by elongation of the interpolar microtubule bundles and no movement of the chromosomes relative to the ends of the spindle. This movement is thus analogous to anaphase B. From +90 to +150 s, it is clear that anaphase B movement is occurring with the chromosomes between microtubule bundles. At +180 and +210 s, the spaces between microtubule bundles became less apparent, and this spindle adopted a filled-in appearance like that described by Dumont *et al.* (2010). We suggest that this apparent change in morphology is a result of spindle narrowing. The spindle width perpendicular to the pole-to-pole axis was reduced from 4.34 µm at anaphase onset (+30 s) to 2.40 µm at +210 s, when spaces between bundles were no longer apparent. The width of interpolar microtubule-poor channels must thus be reduced, making them more difficult to resolve. Thus, in agreement with the fixed-time-point imaging of Muscat *et al.* (2015), our time-lapse imaging revealed that chromosomes are located in microtubule-poor channels throughout anaphase, but the channels can be obscured by narrowing of the spindle.

The outward pushing model of Dumont *et al.* (2010) was supported by the apparent lack of spindle microtubules outside the separating chromosomes. However, under optimal imaging conditions, GFP:tubulin fluorescence signal was observed outside the chromosomes during anaphase (Figure 1B, red arrows at +420 and +495 s; 11/16 time-lapse sequences). This signal appears to indicate the presence of pole-to-pole fibers, as well as additional

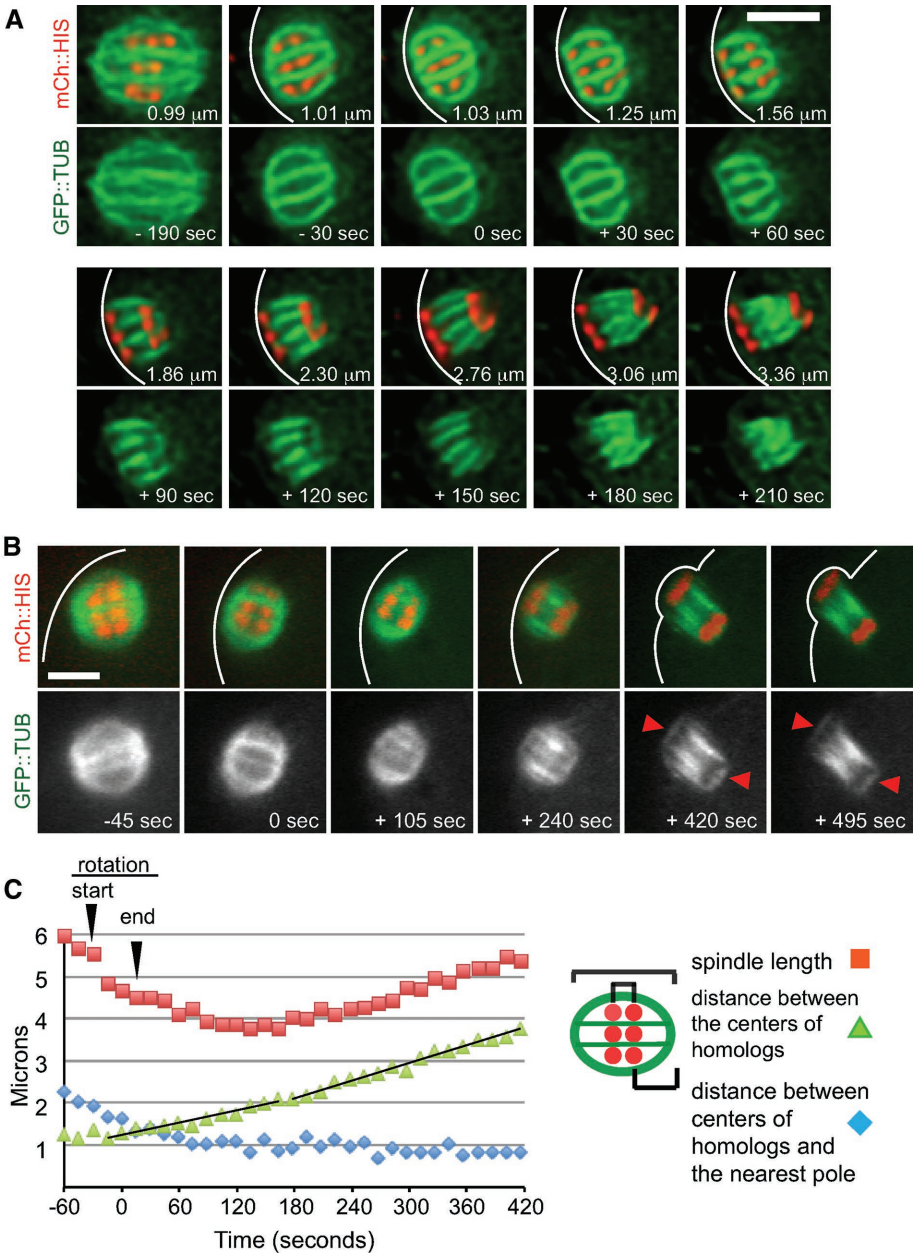

FIGURE 1: Chromosomes initially travel through microtubule-poor channels and then become embedded in the spindle pole. (A) Time-lapse images of an embryo expressing GFP::tubulin and mCherry::histone show an MI metaphase spindle that shortens and rotates (–190 to –30 s) and undergoes anaphase chromosome separation (0 to +210 s). Distances were measured between the centers of homologues, and the average distance between each of the three homologue pairs is shown for each time point. Times are from the start of chromosome separation; white lines indicate the cortex; bar, 4 µm. (B) Time-lapse images of an embryo expressing GFP::tubulin and mCherry::histone show a shortened MI spindle that rotates (–45 to 0 s) and undergoes anaphase A–like chromosome separation (0 to +105 s). At +240 s, the homologues are embedded in the spindle poles and continue to separate as the spindle lengthens. GFP:tubulin signal is clearly visible outside the chromosomes throughout anaphase B (red arrowheads). Times are from the start of chromosome separation; bar, 4 µm; white lines indicate the positions of the cortex. (C) Graph depicting data obtained from the embryo in B.

spindle pole microtubules. Tubulin signal outside the chromosomes was not obvious after +60 s in Figure 1A due to the deconvolution used to enhance the microtubule-poor channels. Thus these results suggest that spindle microtubules are present outside the separating chromosomes, although they can be difficult to image.

To better understand the relative contributions of spindle shortening and anaphase A-like and anaphase B-like movements, we tracked the increase in center-to-center separation of chromosome pairs, pole-to-pole spindle length, and distance between the center of the histone-labeled chromosomes and the outside edge of the GFP::tubulin signal in time-lapse sequences with clear GFP::tubulin signal outside the chromosomes. A plot from a single embryo is shown in Figure 1C, and data from multiple embryos are shown in Figure 2. Anaphase I homologue separation initiated on spindles that averaged 4.08 µm in length and had a starting center-to-center distance between homologues of 1.01 µm. During an initial anaphase A–like movement, both spindle shortening by an average of 0.55 µm and outward homologue separation of 1.13 µm contributed to the decrease in distance between chromosomes and poles (Figures 1C and 2A). Thus, during meiosis I anaphase A–like movement, each pole moved an average of 0.55/2 = 0.28 µm toward the homologues, and each homologue moved 1.13/2 = 0.57 µm toward the pole. After shortening to an average of 3.53 µm, spindles began elongating at the same velocity as chromosome separation (Figures 1C and 2A), indicating an anaphase B–like movement.

Anaphase A and anaphase B typically have distinct velocities (Ris, 1943; Inoué and Ritter, 1978) because they occur by distinct molecular mechanisms (Ris, 1949). As shown in Figure 2, B–D, anaphase A–like chromosome separation had an average velocity of 0.56 µm/min, whereas anaphase B–like chromosome separation had an average velocity of 0.9 µm/min. The anaphase A–like velocities were significantly different from the anaphase B–like velocities, whereas the velocities during anaphase I were not significantly different from those during anaphase II (Figure 2C).

Anaphase A initiates when kinetochore stretching and spindle shortening bring spindle poles into contact with the chromosomes

The short length of the spindle at anaphase onset (4.08 µm; Figure 2A) suggested that chromosomes might already be in physical contact with spindle poles before anaphase onset. Testing this hypothesis requires accurate determination of the inner edges of the spindle poles and the outer edges of the bivalents. To determine the bivalent edges, we conducted time-lapse imaging of ZWL-1::GFP (Figure 3, A and B). ZWL-1 is the *C. elegans* homologue of zwilch, a component of the outer kinetochore during *C. elegans* female meiosis (Dumont *et al.*, 2010) that is required for targeting

A

	Spindle Length (μm)				Distance between Homolog/Sister Centers (μm)			
	MI	n =	MII	n =	MI	n =	MII	n =
Start Anaphase A	4.08 +/- 0.19	15	3.60 +/- 0.11	12	1.01 +/- 0.06	12	0.75 +/- 0.04	12
End Anaphase A	3.53 +/- 0.09	11	3.05 +/- 0.06	13	2.14 +/- 0.09	13	1.83 +/- 0.04	13
Start of cortical Ingression	5.84 +/- 0.24	11	5.49 +/- 0.14	11	4.54 +/- 0.26	14	4.29 +/- 0.21	12

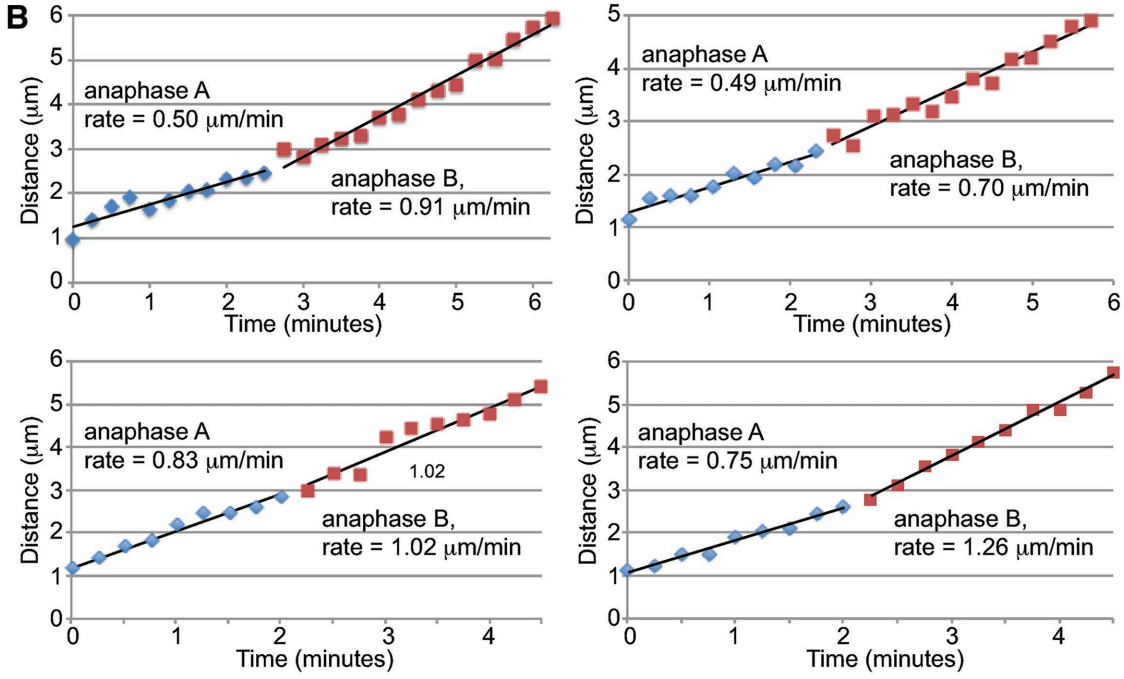

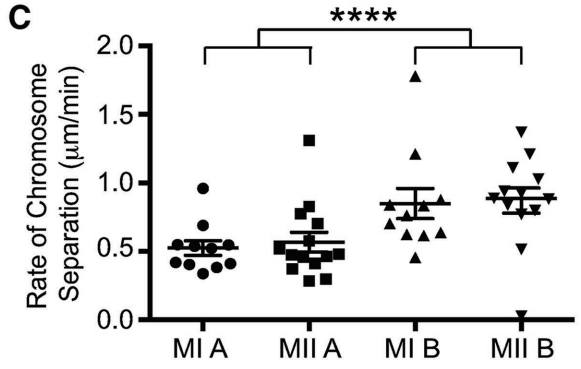

D

Stage	Rate	S.E.M.	n
All anaphase A	0.56	0.05	25
All anaphase B	0.90	0.06	24
MI anaphase A	0.52	0.05	11
MII anaphase A	0.58	0.07	15
MI anaphase B	0.85	0.11	11
MII anaphase B	0.95	0.06	13

FIGURE 2: *C. elegans* meiosis has both anaphase A and anaphase B. (A) Table of spindle lengths and distances between the centers of chromosomes measured at the start of anaphase A, the end of anaphase A, and the start of cortical ingression for both MI and MII meiotic spindles. Averages and SEM (B) Graphs depicting the change in distance between separating chromosomes in time-lapse sequences of four embryos show different rates during anaphase A and anaphase B. (C) Rates of chromosome separation from multiple time-lapse sequences of MI anaphase A, MII anaphase A, MI anaphase B, and MII anaphase B. Although there is no significant difference between MI and MII rates, the difference between all anaphase A rates and all anaphase B rates is extremely significant (****$p < 0.0001$). (D) Table of the averages of the rates shown in C. All rates were determined from time-lapse images of embryos expressing GFP::tubulin and mCherry::histone and are expressed as micrometers/minute.

dynein to kinetochores during prometaphase in *C. elegans* (Gassmann *et al.*, 2008) and other species (Starr *et al.*, 1998; Griffis *et al.*, 2007; Raaijmakers *et al.*, 2013). In addition to labeling the cup-shaped kinetochores, ZWL-1 became transiently associated with spindle poles during spindle rotation (Figure 3B, –60 s). The tips of the kinetochore cups came into contact with the spindle poles (Figure 3B, –30 s) and then merged with the spindle poles (Figure 3B, 0 s) before any increase in the gap between homologues. The spindle continued to shorten during anaphase A as the ZWL-1 became undetectable (Figure 3B, +60 s). Contact between the poles and kinetochores was driven by both spindle shortening and an increase in the length of the bivalents. Analysis of a single

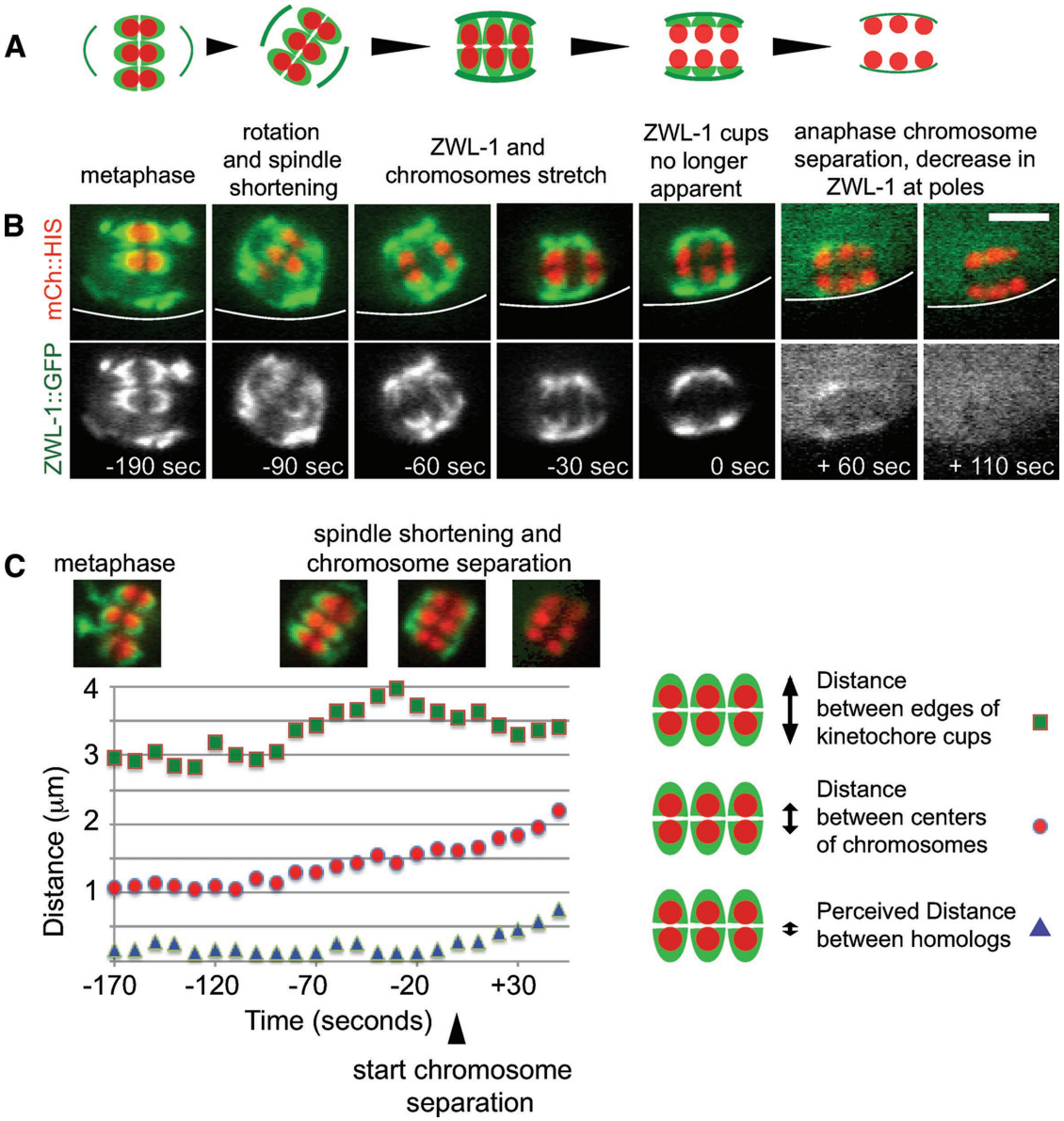

FIGURE 3: Kinetochore cups merge with poles during spindle shortening and then disappear as chromosomes separate. (A) Cartoon interpretation of data in B and C and showing ZWL-1::GFP on kinetochores and spindle poles. Kinetochores and chromosomes stretch as the spindle shortens. ZWL-1::GFP on kinetochore cups then appears to merge with ZWL-1::GFP on the spindle pole; ~20 s after this merge, chromosomes begin to visibly separate, and ZWL-1::GFP fluorescence fades. (B) Time-lapse images of an embryo expressing ZWL-1::GFP and mCherry::histone show an MI metaphase spindle that shortens (–90 to +60 s), rotates (–60 to –30 s), and undergoes anaphase A chromosome separation (0 to +110 s). Brightness and contrast were altered on +60 and +110 images due to the decrease in ZWL-1::GFP fluorescence. Times are from the start of chromosome separation; white lines indicate the cortex. Bar, 4 µm. (C) Data from time-lapse images of a single MI embryo expressing ZWL-1::GFP and mCherry::histone. For each time point, measurements were made on the homologue pair that was most clearly in focus. Times are from the start of chromosome separation. Representative images are above the graph.

time-lapse sequence (Figure 3C) revealed that the tip-to-tip distance between the ends of the ZWL-1 cups of meiosis I bivalents increased at a faster velocity than the increase in distance between the centers of the homologues (Figure 3C, –70 to –20 s), indicating that the bivalents are stretched outward before cleavage of cohesin. The average distance between the tips of ZWL-1 cups increased from 3.09 µm at metaphase to 4.05 µm just before the initiation of an increased gap between homologues (Figure 4, A and B). This distance is similar to the average spindle length at the onset of anaphase A determined from GFP::tubulin, 4.08 µm (Figure 2A). Thus the outer edges of bivalents clearly merge with spindle poles before a measurable increase in the gap between homologues.

To distinguish more rigorously whether the outward movement of kinetochores is due to chromatin stretching before cohesin cleavage or chromosome movement after cohesin cleavage, we measured the distance between the tip of one ZWL-1 cup

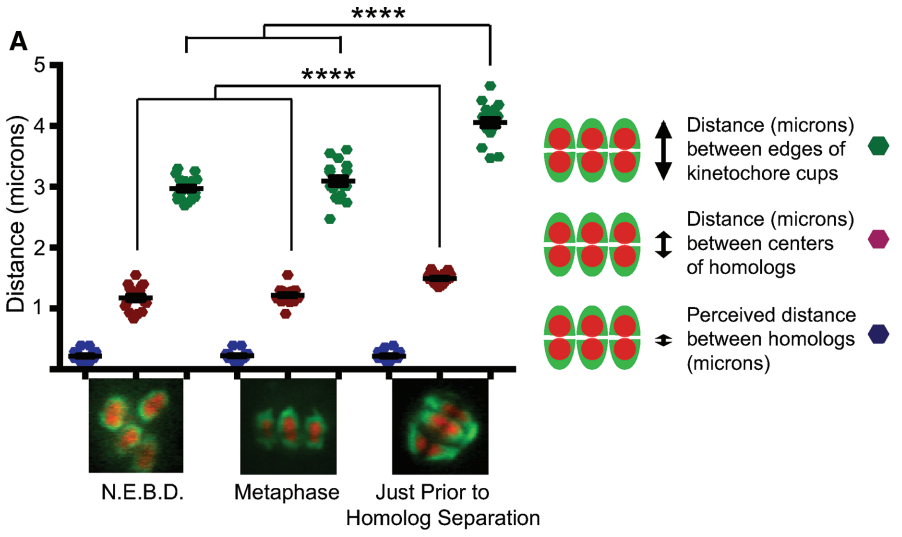

B

Average Distance (microns)

Stage	Between Edges of ZWL-1	n	Between Centers of Homologs	n	Separation of Homologs	n
N.E.B.D.	2.97 +/- 0.04	18	1.17 +/- 0.05	18	0.21 +/- 0.02	18
Metaphase	3.09 +/- 0.08	18	1.22 +/- 0.02	18	0.22 +/- 0.02	18
Just Prior to Homolog Separation	4.05 +/- 0.07	18	1.46 +/- 0.03	18	0.22 +/- 0.02	18

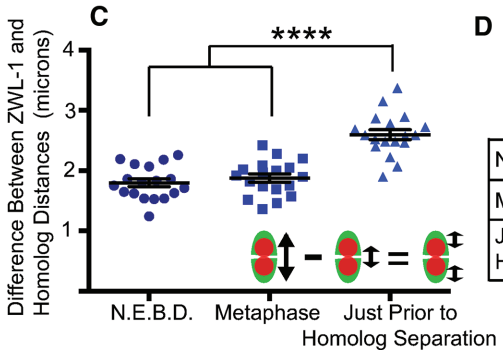

D

Average Difference Between ZWL-1 Distances and Homolog Distances (microns)

Stage		n
N.E.B.D.	1.80 +/- 0.07	18
Metaphase	1.88 +/- 0.07	18
Just Prior to Homolog Separation	2.60 +/- 0.08	18

FIGURE 4: Chromosomes and kinetochores stretch immediately before the start of homologue separation. (A) Differences in the size of homologue and kinetochore pairs at difference stages of meiosis determined from time-lapse sequences of ZWL-1::GFP and mCherry::histone. N.E.B.D., nuclear envelope breakdown. "Just prior to Homolog Separation" is the frame immediately preceding an increase in the apparent gap between homologues (–20 s in Figure 3C). ****$p < 0.0001$, extremely significant difference. (B) Averages and SEM for the data in A. (C) Differences between ZWL-1 and homologue distances for each of the 56 chromosome pairs in A and B. The differences increase just before homologue separation, indicating that, although both kinetochores and chromosomes stretch before homologue separation, the kinetochores stretch to a greater extent. ****$p < 0.0001$. (D) Averages and SEM for the data in C.

and the center of its corresponding mCherry:histone–labeled homologue. This distance increased significantly between metaphase and the time point just before an increase in the gap between homologues (Figure 4, C and D). The center-to-center distance between histone-labeled homologues also increased slightly between these time points (1.22 to 1.46 µm; Figure 4B), indicating stretching of the chromatin as well as of the ZWL-1. These results support a model in which bivalents are stretched outward and meet the inwardly approaching poles just before cohesin cleavage.

Chromosomes are embedded in spindle poles during anaphase B

The analyses in Figures 1 and 2, which use the outside edge of GFP::tubulin as an indicator of the spindle pole, do not take into account the thickness of the pole. We therefore tracked the relative positions of chromosomes and GFP::ASPM-1, which labels poles throughout meiosis. Analysis of a single time-lapse sequence (Figure 5B) is shown in Figure 5C, and average data are summarized in Figure 5D. GFP::ASPM-1–labeled poles moved inward toward chromosomes so that at anaphase onset, the distance between the center of the spindle (midpoint between the homologues) and the inner edge of the GFP::ASPM-1 averaged 1.35 µm (Figure 5, C and D). The distance between the center of the spindle and the outside edge of ZWL-1::GFP averaged 2.02 µm (Figure 4B; 4.05/2). Thus the inner edge of GFP::ASPM-1 overlapped with the outer edge of ZWL-1::GFP at anaphase onset (Figure 5D). During an anaphase A–like movement, spindle poles continued to move inward as homologues moved a short distance outward (Figure 5, B and C, 0–100 s). Finally, during anaphase B, homologues were embedded in the GFP::ASPM-1 as both chromosomes and poles separated (Figure 5, B and C, 100–200 s).

Both anaphase A and anaphase B are unaffected by dynein depletion, and dynein dissociates from kinetochores before initiation of anaphase

To test whether dynein is the primary motor responsible for anaphase A, as proposed by Muscat *et al.* (2015), we depleted DHC-1 by RNA interference (RNAi) to the maximum extent possible that still allowed time-lapse imaging of anaphase chromosome movement on spindles with two distinct poles. Whereas *dhc-1(RNAi)* spindles had a number of structural defects during prometaphase (Figure 6A, 9.25 min) and failed in spindle rotation and polar body formation (Figure 6A, 0.5–6.25 min), they shortened (Figure 6A, 1.0 and 14.0 min; Yang *et al.*, 2005), and anaphase still occurred (Figure 6A). We measured the chromosome separation rate before and after the chromosomes reached the edge of the GFP::tubulin–labeled spindle. Although we observed lagging chromosomes (Figure 6A, 15.0 min) like those described by Muscat *et al.* (2015), the average velocity of the separating chromosomes was not reduced relative to controls during anaphase A– or B–like movement (Figure 6, B and C). This result indicated that either dynein is not the primary anaphase motor or anaphase requires a threshold concentration of dynein that is below the concentration required for bipolar spindle assembly.

Because we could not detect a reduction in anaphase velocity upon dynein depletion, we tested whether dynein is present on

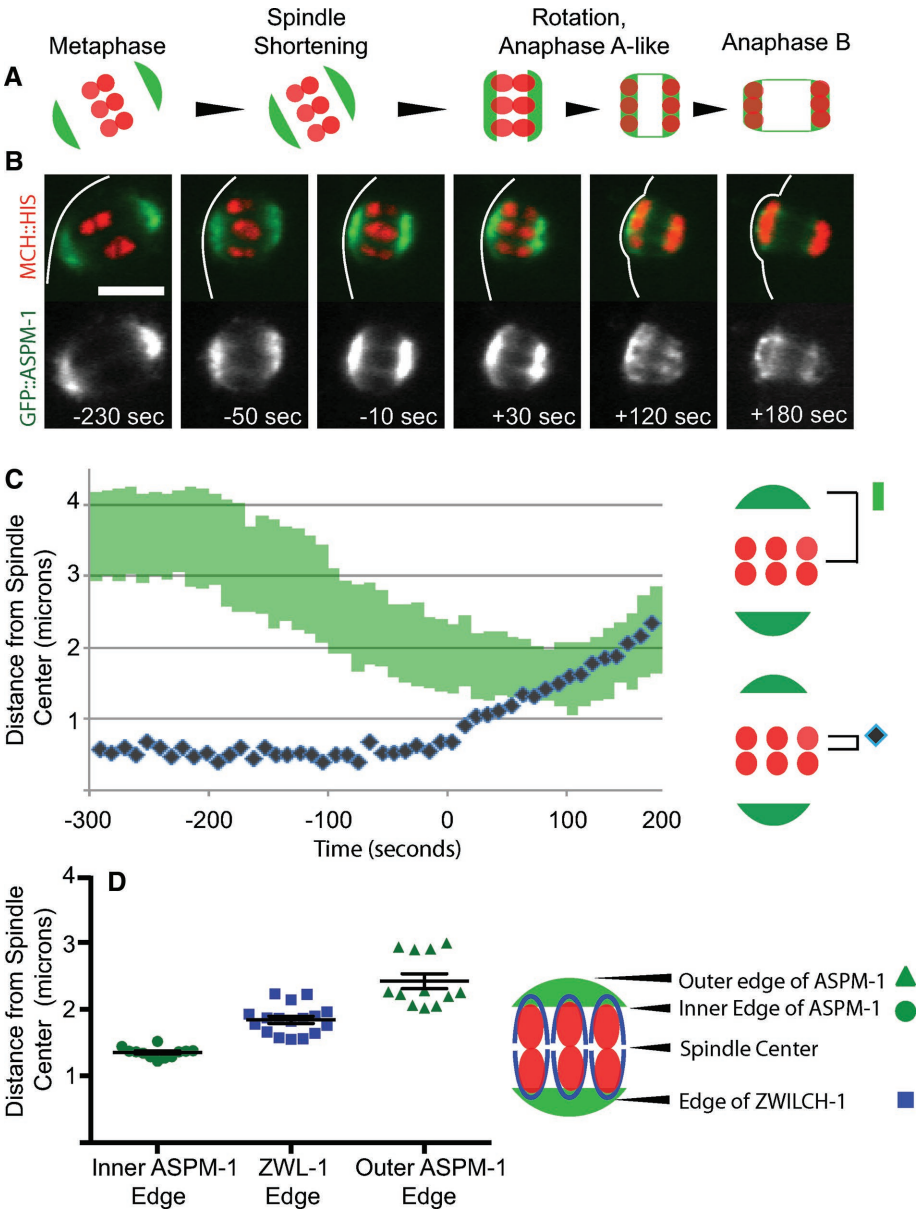

FIGURE 5: Chromosomes come into close contact with GFP::ASPM-1 on spindle poles during spindle shortening and then become embedded in the ASPM-1 during anaphase B separation. (A) Cartoon model showing GFP::ASPM-1 slightly overlapping chromosomes just before anaphase A separation and then fully overlapping them during anaphase B. (B) Representative time-lapse sequence from an MI embryo expressing GFP::ASPM-1 and mCherry::histone shows the spindle shorten and rotate (−230 to −10 s) and undergo anaphase A and anaphase B chromosome separation (0 to +180 s). Holes in the GFP::ASPM fluorescence that correspond to the pole-embedded chromosomes are visible at 120 and 180 s. White lines indicate the cortex. Bar, 5 μm. (C) Change in the position of homologues with respect to the ASPM-rich pole as the homologues separate. The depth of the green bars indicates the thickness of GFP::ASPM-1 on the spindle pole. By 100 s, the chromosomes have become embedded in the pole material. Times are from the start of chromosome separation in B and C. (D) Relationship between outermost edges of kinetochores and ASPM-rich poles immediately before chromosome segregation in MI anaphase.

kinetochores during anaphase chromosome movement. In a fraction of time-lapse sequences of GFP::DHC-1, dynein was discernible on the cup-shaped kinetochores during prometaphase and metaphase (Figure 7, A, −100 s, and B, −150 s). However, in 10 of 11 time-lapse sequences in which dynein was detectable at prometaphase, this signal was lost before initiation of chromosome separation (Figure 7A, 0 s). Just before spindle rotation, dynein accumulated at spindle poles that were clearly separate from the chromosomes (Figure 7A, 0 s) before the spindle shortened to juxtapose the poles against the chromosomes (Figure 7, A, 20 s, and B, 10 s). During anaphase B, chromosomes were clearly embedded within the dynein-labeled spindle poles (Figure 7, A, 90 s, and B, 190 s). The extremely low signal-to- noise ratio of GFP::DHC-1 at kinetochores of wild-type bipolar spindles made it difficult to prove that dynein is removed from kinetochores before anaphase onset. However, dynein requires ZWL-1 for targeting to prometaphase kinetochores in *C. elegans* (Gassmann *et al.*, 2008), and ZWL-1 no longer labeled cup-shaped kinetochores at anaphase onset (Figure 3B, 0 s). These data are consistent with the hypothesis that dynein dissociates from kinetochores before anaphase onset as described in other cell types and suggest that the dynein on the leading edge of anaphase chromosomes described by Muscat *et al.* (2015) is in fact spindle pole dynein rather than kinetochore dynein.

Depletion of dynein results in spindles that are longer than wild type at metaphase (Ellefson and McNally, 2011), leaving the possibility that spindle shortening in dynein-depleted embryos might not be sufficient to bring poles into contact with chromosomes. However, imaging of GFP:ASPM-1 in dynein-depleted embryos (Figure 7C) revealed that GFP:ASPM-1–labeled poles still achieve close proximity to chromosomes before anaphase onset.

Anaphase B requires the doublecortin family member ZYG-8

Anaphase B should theoretically require net plus-end polymerization to maintain the antiparallel overlap of interpolar microtubule bundles. Loss of the doublecortin family member ZYG-8 was previously shown to reduce microtubule polymerization rate (Srayko *et al.*, 2005) and prevent the anaphase-specific elongation of astral microtubules during mitosis (Gönczy *et al.*, 2001). We therefore hypothesized that ZYG-8 might be required for anaphase B during meiosis. Time-lapse imaging of GFP:tubulin and mCherry:histone in a *zyg-8(ts)* mutant at nonpermissive temperature (Figure 8, A and B) revealed that meiotic spindles exhibited minimal elongation from an average minimum length of 4.01 μm to only 4.22 μm, in contrast with control spindles, which elongated from a minimum length of 3.51 μm to 5.85 μm (Figure 8C). The average chromosome separation rate in *zyg-8* mutant embryos (0.43 μm/min; Figure 8C) was more similar to the rate of anaphase A (0.56 μm/min) than that of anaphase B (0.90 μm/min) in control

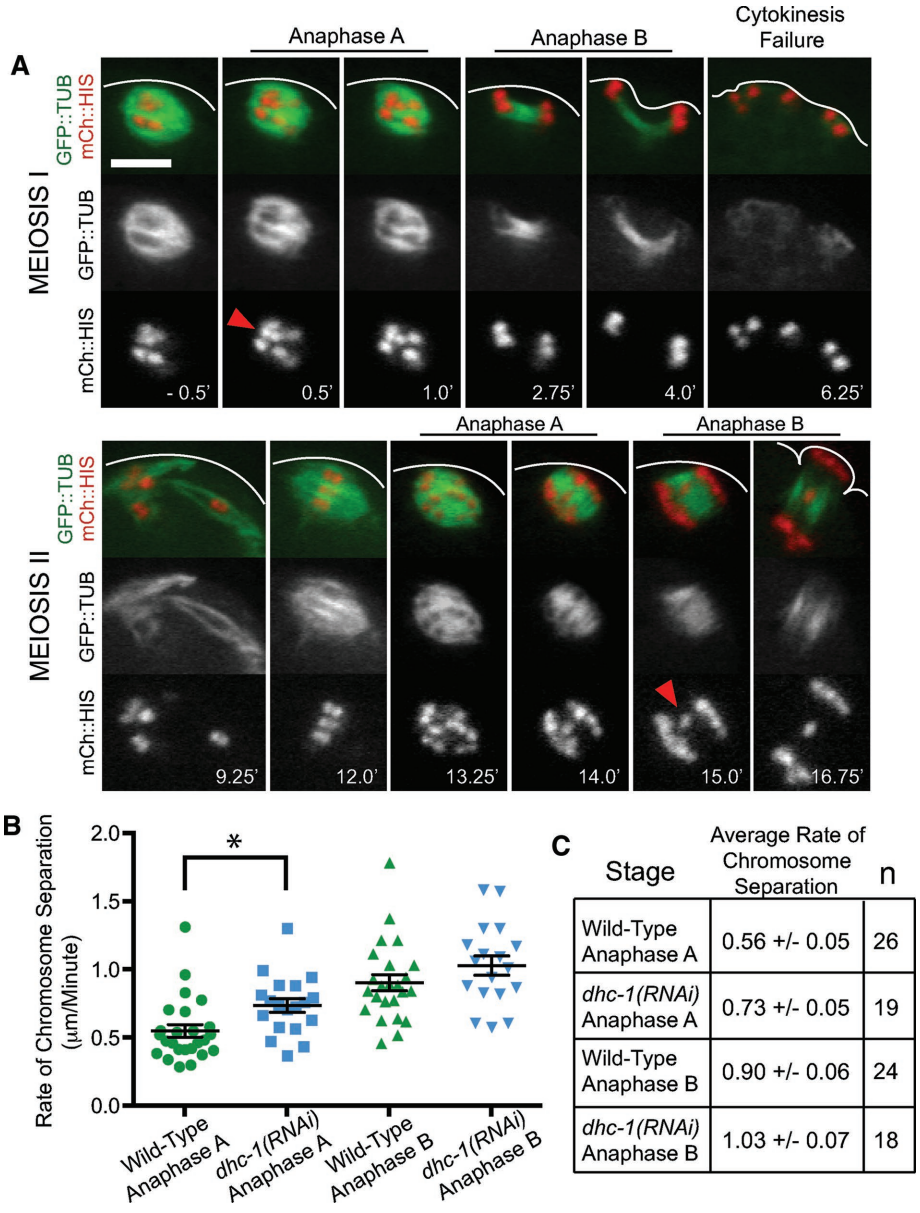

Stage	Average Rate of Chromosome Separation	n
Wild-Type Anaphase A	0.56 +/- 0.05	26
dhc-1(RNAi) Anaphase A	0.73 +/- 0.05	19
Wild-Type Anaphase B	0.90 +/- 0.06	24
dhc-1(RNAi) Anaphase B	1.03 +/- 0.07	18

FIGURE 6: Depletion of DHC-1 does not decrease the rate of either anaphase A or B. (A) Time-lapse images of an embryo expressing GFP::tubulin and mCherry::histone and depleted of DHC-1 were captured during both MI and MII. The shortened spindle at –0.5 min fails to rotate and undergoes chromosome separation parallel to the cortex. MI polar body formation fails, and the MII spindle captures all 12 univalents as it forms (9.25 min). The MII spindle shortens but fails to rotate, and chromosome separation occurs at a slight angle to the cortex (13.25–15.0 min). At 16.75 min, the cortex has "captured" the sister chromatids that are closest, and polar body formation has begun. Lagging chromosomes (red arrowheads) are observed in both anaphase I and II. Times are from start of MI chromosome separation. (B) Rates of chromosome separation were determined during anaphase A and B in both wild-type and DHC-1– depleted embryos. Data for anaphase I and anaphase II were combined since they are not significantly different. *$p < 0.05$. (C) Average rates and SEM for each of the four conditions. Bar, 5 µm.

embryos. Thus a protein required to increase the rate of plus-end polymerization and increase the length of microtubules during anaphase is required for anaphase B during *C. elegans* meiosis, consistent with an outward sliding mechanism.

In many organisms, the bipolar kinesin 5 drives anaphase B; however, loss of the *C. elegans* kinesin 5, BMK-1, results in faster anaphase B during mitosis in the one-cell embryo (Saunders *et al.*, 2007). To test the role of BMK-1 in outward sliding during *C. elegans* meiosis, we carried out time-lapse imaging of GFP::tubulin and mCherry::histone in worms carrying *bmk-1(ok391)*, a recessive reduction-of-function allele (Connolly *et al.*, 2014). The velocity of anaphase B was 0.96 ± 0.07 µm/min ($n = 14$), which is not significantly different from that for controls ($p = 0.52$). Thus BMK-1 neither promotes nor resists anaphase B outward sliding during *C. elegans* female meiosis.

Spindle pole movement toward chromosomes contributes to anaphase during female meiosis in *Spisula solidissima*

To test whether movement of spindle poles toward chromosomes during female meiosis occurs in other animal phyla, we analyzed the fertilized zygotes of *Spisula solidissima*, phylum Mollusca, by fixed anti-tubulin immunofluorescence (Figure 9A). Metaphase I average spindle length was significantly greater than anaphase average spindle length (metaphase I, 14.8 ± 0.5 µm, $n = 24$; anaphase I, 9.2 ± 0.6, $n = 12$; $p < 0.0001$). To interpret the large variation in spindle lengths in fixed images, we plotted pole-to-pole spindle length against the distance between homologues (Figure 9B). For the anaphase spindles, there was a positive correlation between spindle length and homologue separation distance (Pearson $r = 0.83$), indicating that anaphase B contributes to chromosome segregation. Metaphase spindles had a wide range of lengths, with the shortest lengths approaching those of the shortest anaphase spindles (Figure 9B). We interpret that the longest, 20 µm, metaphase spindles as being the earliest spindles because prophase nuclei average >40 µm in diameter (Figure 9, C and D), and the centrosomes separate around the nucleus during prophase (Figure 9E). These measurements are consistent with a model in which spindles are 20 µm long at the beginning of metaphase and shorten to 8 µm to bring poles into close proximity to the homologues. The poles then separate in an anaphase B–like process.

DISCUSSION

A model for kinetochore-independent anaphase

We present a model of *C. elegans* female meiotic chromosome segregation based on the quantitative measurements reported here (Figure 10). Spindle shortening and outward stretching of bivalents result in physical overlap and tethering of the outer edges of bivalents to spindle poles before loss of cohesion (Figure 10B). Outward sliding of interpolar microtubule bundles then moves spindle poles and their bound chromosomes apart in an anaphase

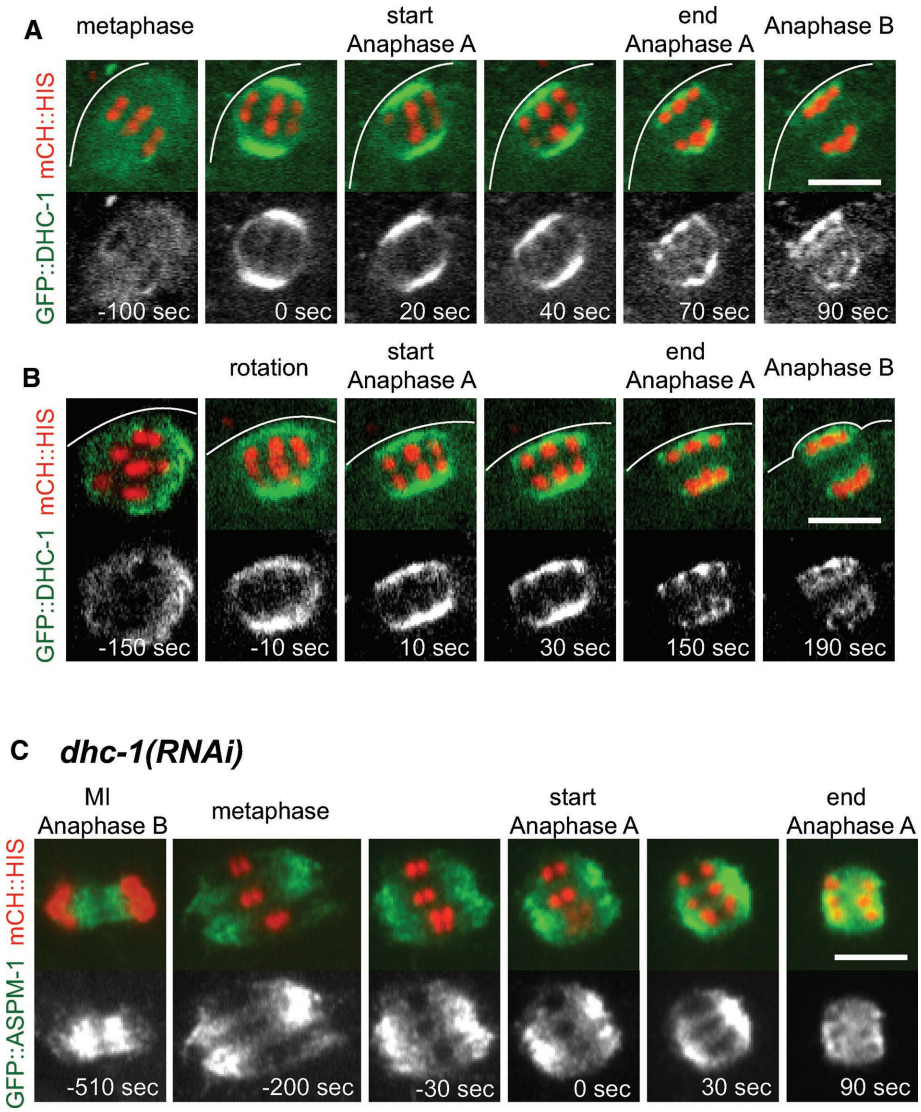

FIGURE 7: Dynein dissociates from kinetochores before chromosome separation. (A) Time-lapse images of an MI embryo expressing GFP::DHC-1 show DHC-1 on kinetochores during metaphase (–100 s). DHC-1 disappears from kinetochores and concentrates on the spindle pole during shortening and anaphase A (0–40 s). (B) Time-lapse images of a second MI embryo show that DHC-1 on the spindle pole encircles the chromosomes during anaphase B (150–190 s). Times are from the start of chromosome segregation; white lines indicate cortices; bars, 5 µm. (C) Time-lapse images of a DHC-1–depleted embryo expressing GFP::ASPM-1 and mCherry::histone. The images show an MII spindle (–200 s), which shortens (–30 to 0 s), does not rotate, and undergoes anaphase A chromosome segregation (30–90 s). Times are from the start of chromosome segregation. Bar, 5 µm.

B–like movement. The kinetochore proteins KNL-1 (Dumont *et al.*, 2010) and ZWL-1 (this study) dissociate from chromosomes during this handoff of chromosomes to the spindle poles. Depletion of KNL-1 had little effect on the velocity of anaphase (Dumont *et al.*, 2010) because spindle shortening is sufficient to bring homologues into contact with their spindle pole attachment sites. Prometaphase orientation of bivalents within the microtubule-poor channels between interpolar microtubule bundles is completely dependent on the kinetochore protein KNL-1, which is required for kinetochore targeting of both NDC-80 complex and ZWL-1 (Dumont *et al.*, 2010). We therefore hypothesize that orientation and stretching of bivalents is mediated by NDC-80 complex, KNL-1, RZZ-coupled dynein, and possibly other KNL-1–dependent microtubule-interacting proteins on the kinetochore cups. This hypothesis is supported by the observation of aneuploid metaphase II spindles in KNL-1–depleted embryos (Dumont *et al.*, 2010).

Whether outer kinetochore proteins generate outward pulling force through lateral or end-on microtubule attachments cannot be discerned from imaging alone, as the presence of dense interpolar microtubule bundles does not exclude the existence of lower-density microtubules within the microtubule-poor channels. However, in vitro studies indicate that the NDC-80 complex generates force through end-on attachment (Powers *et al.*, 2009), and dynein can generate force through lateral or end-on attachment (Mallik *et al.*, 2004; Laan *et al.*, 2012).

We hypothesize that spindle shortening is driven by inward sliding by kinesin 14 family members because these kinesins oppose kinesin 5–mediated outward sliding in other organisms (Saunders *et al.*, 1997; Mountain *et al.*, 1999; Sharp *et al.*, 1999). Because there are four, potentially redundant kinesin 14 family members in *C. elegans*—KLP-15, KLP-16, KLP-3, and KLP-17—this hypothesis has been difficult to test.

If anaphase A occurs as KNL-1 (Dumont *et al.*, 2010) and ZWL-1 (this study) are dissociating from chromosomes, what mechanisms might drive anaphase A after the handoff of chromosomes from kinetochores to spindle poles? The centers of histone-labeled chromosomes move 1.13 µm apart during anaphase A–like movement, which means that the center of each homologue only moves 1.13/2 = 0.56 µm through the microtubule-poor channels. Because bivalents are 4.0 µm long when we propose that cohesin is cleaved, anaphase A occurs over a fraction of a chromosome length. We suggest two noncanonical mechanisms that could contribute to this short-range motion. Because experimentally stretched chromosomes return to their original shape when tension is released (Paliulis and Nicklas, 2004) and *C. elegans* bivalents are stretched by 1 µm (Figure 3), cleavage of cohesin could generate 1 µm of chromosome separation by elastic recoil of the chromatin (Figure 10C). A second noncanonical mechanism is suggested by the spherical spindle shape generated by spindle shortening (Crowder *et al.*, 2015). Interpolar microtubule bundles are clearly bent into a semicircular shape by spindle shortening and straighten during anaphase (Figure 1A). For a spherical spindle with a length of 4.0 µm, the length of one interpolar bundle is actually $0.5(2\pi r) = \pi(2\ \mu m) = 6.2\ \mu m$. Straightening of the microtubule bundles could move chromosomes tethered to the ends of the spindle by 6.2 – 4 = 2.2 µm apart. Because it takes piconewton (pN) forces to bend a single GDP microtubule in vitro with an optical trap and these bent microtubules return to a straight conformation upon release of force

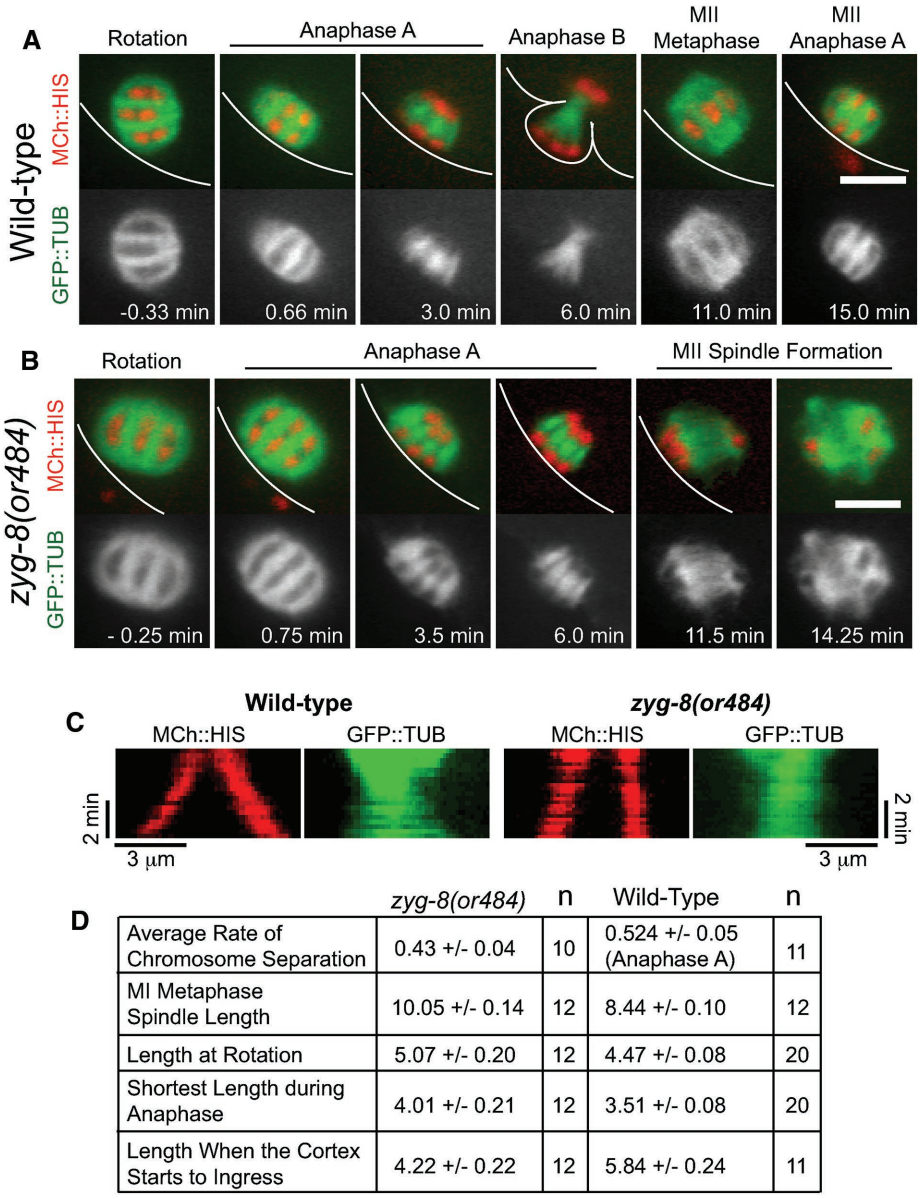

D

	zyg-8(or484)	n	Wild-Type	n
Average Rate of Chromosome Separation	0.43 +/- 0.04	10	0.524 +/- 0.05 (Anaphase A)	11
MI Metaphase Spindle Length	10.05 +/- 0.14	12	8.44 +/- 0.10	12
Length at Rotation	5.07 +/- 0.20	12	4.47 +/- 0.08	20
Shortest Length during Anaphase	4.01 +/- 0.21	12	3.51 +/- 0.08	20
Length When the Cortex Starts to Ingress	4.22 +/- 0.22	12	5.84 +/- 0.24	11

FIGURE 8: The doublecortin family member ZYG-8 is required for anaphase B. Time-lapse images of control (A) or *zyg-8(ts)* (B) embryos expressing GFP::tubulin and mCherry::histone. The *zyg-8(ts)* MI spindle does not elongate after anaphase A. Times are from the start of chromosome segregation; bars, 5 μm. (C) Kymograph analysis of chromosome separation in time-lapse sequences from a wild-type embryo and a *zyg-8(ts)* embryo incubated at the restrictive temperature. Start times are at the completion of spindle rotation. (D) Data obtained from *zyg-8(ts)* embryos incubated at the restrictive temperature and from wild-type embryos examined under similar conditions.

(Kikumoto *et al.*, 2006), we suggest that cohesin cleavage would allow microtubules to return to a straight conformation, resulting in pN forces on chromosomes tethered to the ends of the microtubules. Chromosomes separate by <2 μm because the spindle continues to shorten during anaphase A.

We suggest that, once chromosomes overlap the ASPM-labeled poles, the kinesin 12 family member kinesin-like protein (KLP)-18 provides the major outward sliding force during anaphase B. This hypothesis is based on the observation that KLP-18 depletion results in monopolar meiotic spindles (Wignall and Villeneuve, 2009), just as strong depletion of kinesin 5 results in monopolar spindles in other species (Heck *et al.*, 1993; Mountain *et al.*, 1999). In addition, mammalian kinesin 12 acts redundantly with kinesin 5 in vivo (Tanenbaum *et al.*, 2009), suggesting that they act by similar mechanisms. Kinesin-5 motors are responsible for separating duplicated poles by virtue of their antiparallel tetrameric structure, which allows them to bundle and slide parallel and antiparallel microtubules (Kapitein *et al.*, 2005; Tao *et al.*, 2006; Scholey *et al.*, 2014). Mammalian kinesin 12 can also cross-link and slide both antiparallel and parallel microtubules (Drechsler and McAinsh, 2016). We suggest that, at the end of anaphase A, chromosomes become physically tethered to the poles; KLP-18 then slides antiparallel microtubules apart during anaphase B, whereas ZYG-8–driven microtubule polymerization maintains microtubule overlap (Figure 10, D and E). The microtubule dynamics regulator CLS-2, which is required for anaphase (Dumont *et al.*, 2010), may also contribute to maintaining antiparallel overlap.

How might chromosomes be tethered to spindle poles? *C. elegans* katanin, composed of MEI-1 and MEI-2 subunits, colocalizes with meiotic chromosomes during metaphase (Srayko *et al.*, 2000; McNally *et al.*, 2014), suggesting that it can bind chromatin. Katanin is also found at spindle poles throughout meiosis, and time-lapse imaging revealed GFP::MEI-1 on chromosomes merging with GFP::MEI-1 on poles as spindles shorten to their shortest length (McNally *et al.*, 2006). In addition, strong loss of function of MEI-1 results in spindles with no ASPM-labeled poles (McNally and McNally, 2011; Connolly *et al.*, 2014) and no organized chromosome movement (Yang *et al.*, 2003; Connolly *et al.*, 2014). Recent proteomics work indicates that in human cells, katanin forms complexes with NuMA/LIN-5 and ASPM (Cheung *et al.*, 2016), both of which are concentrated at *C. elegans* meiotic spindle poles (van der Voet *et al.*, 2009). Although anaphase still occurs in ASPM-depleted meiotic embryos (Connolly *et al.*, 2014), these experiments may have been conducted in a partial-loss-of-function state. At mammalian mitotic spindle poles, katanin (McNally and Thomas, 1998), NuMA (Lydersen and Pettijohn, 1980), and ASPM (Higgins *et al.*, 2010) are dispersed by microtubule-depolymerizing drugs. In addition, katanin (McNally *et al.*, 2014) and *Drosophila* ASPM (Ito and Goshima, 2015) can cross-link microtubules in vitro, and we find microtubules at meiotic spindle poles (Figure 1B). We suggest that a complex of katanin, ASPM, NuMA/LIN-5, and cross-linked microtubules both form the spindle pole and capture chromosomes.

The apparent switch from chromosome attachment to the kinetochore to chromosome attachment to the spindle pole may have evolved because of the need to completely reposition kinetochores between meiosis I and II in *C. elegans*. The cup-shaped meiosis I kinetochore envelops two sister chromatids, whereas the cup-shaped

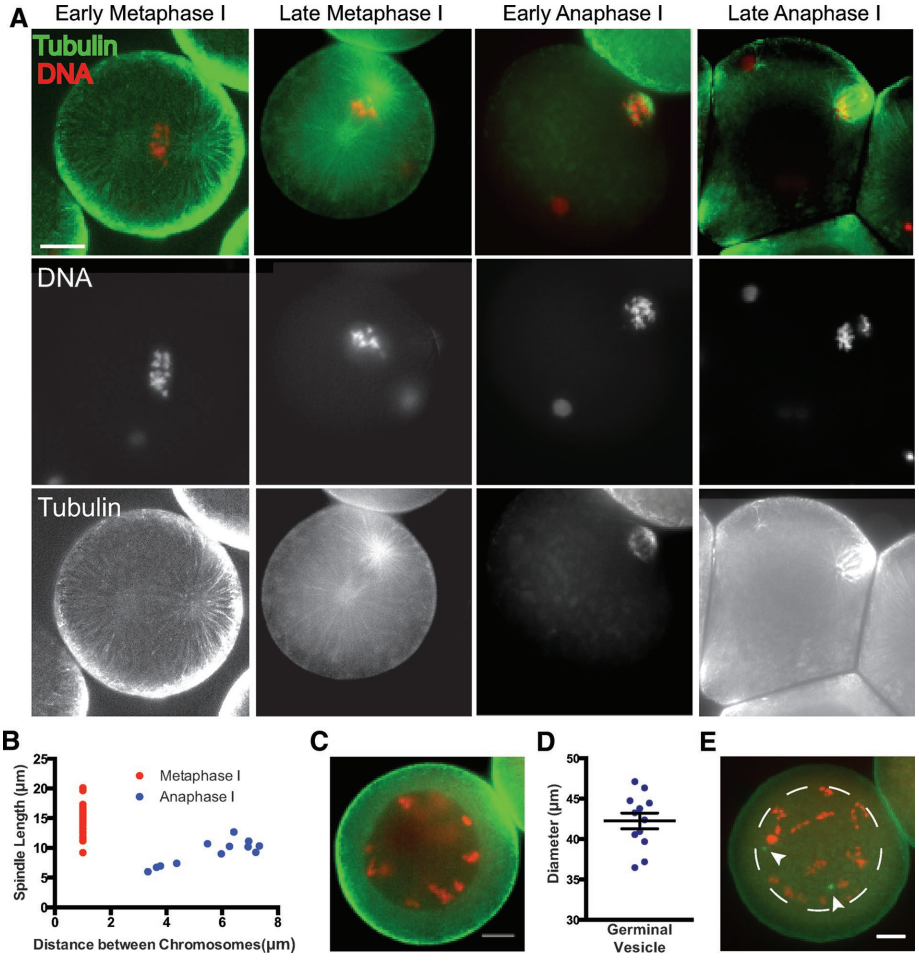

FIGURE 9: Spindle poles move toward chromosomes during meiotic anaphase in *S. solidissima*. (A) Maximum intensity projections of fixed-immunofluorescence images of fertilized *Spisula* embryos stained with DAPI and anti–α-tubulin antibodies. (B) Relationship between spindle length (pole-to-pole distance) and distance between chromosomes in metaphase I ($n = 24$) and anaphase I ($n = 12$). For anaphase I, Pearson $r = 0.8269$. (C) Maximum intensity projection of a *Spisula* zygote at germinal vesicle stage stained with DAPI (red) and α-tubulin (green), which is excluded by the nucleus. (D) Quantification of the germinal vesicle diameter just after fertilization. (E) Maximum intensity projection of a *Spisula* zygote at germinal vesicle stage stained with DAPI (red) and γ-tubulin (green), showing separation of centrosomes across the nuclear surface. The dotted line highlights the nuclear envelope. Bar, 10 µm.

meiosis II kinetochore must envelop only a single sister chromatid. The removal of KNL-1 (Dumont *et al.*, 2010) and ZWL-1 (this study) from kinetochores during anaphase I may be necessary to allow reassembly of the meiosis II kinetochore in a new location. Kinetochore disassembly may then have necessitated a new mechanism for tethering chromosomes to outwardly separating spindle poles.

MATERIALS AND METHODS

C. elegans strains

We used the following strains. FM125: unc-119(ed3); ruIs57[pAZ147:pie-1/β-tubulin::GFP; unc-119(+)]; itIs37 [unc-119(+) pie-1::mCherry::H2B]), FM49: zyg-8(or484ts) III; unc-119(ed3); ruIs57[pAZ147:pie-1/β-tubulin::GFP; unc-119(+)]; itIs37 [unc-119(+) pie-1::mCherry::H2B], EU1561: orIs17[dhc-1::GFP::DHC-1; unc-119(+)]; itIs37[unc-19(+) pie-1::mCherry::H2B], EU2933: itIs37[unc-19(+) pie-1::mCherry::H2B]; or1935[GFP::aspm-1] I, OD1870: ltIs1003[pTK048; Pmex-5::ZWL-1::GFP::tbb-2 3′UTR::operon linker::mCherry:his-58::tbb-2 3′UTR; cb-unc-119(+)]I, and FM387: unc-119(ed3); ruIs57[pAZ147:pie-1/β-tubulin::GFP; unc-119(+)]; itIs37 [unc-119(+) pie-1::mCherry::H2B]; bmk-1(ok391) made by crossing FM125 with SV1005 bmk-1(ok391) V, an 8× outcrossed version of bmk-1(ok391) (Maia *et al.*, 2015), which is a recessive reduction-of-function allele (Connolly *et al.*, 2014).

RNA interference

All of the RNAi experiments were performed by feeding bacteria (HT115) induced to express double-stranded RNA corresponding to each gene as described by Timmons *et al.* (2001) and Kamath *et al.* (2001). L4 hermaphrodites were transferred to RNAi plates and allowed to feed on the RNAi bacterial lawn for 16–24 h. We used *dhc-1* clone I-1PO4 from the genomic RNAi feeding library (Medical Research Council Gene Services, Source BioScience, Nottingham, UK; Kamath *et al.*, 2001).

Live in utero imaging

Adult hermaphrodites were anesthetized with tricaine/tetramisole as described (Kirby *et al.*, 1990; McCarter *et al.*, 1999) and gently mounted between a coverslip and a thin 3% agarose pad on a slide. Images in Figure 1A were captured on an Olympus IX81 microscope equipped with a 60× PlanApo 1.42 oil objective and an ORCA Flash 4.0 CMOS camera (Hamamatsu Photonics, Bridgewater, NJ). All other live images were captured with a PerkinElmer-Cetus Ultraview Spinning Disk Confocal equipped with an Orca R2 CCD and an Olympus 100× 1.35 oil objective. Images in Figure 1A were deconvolved using Huygens Professional X11 (SVI, Hilversum, Netherlands). Deconvolutions were run up to 40 iterations using classic maximum likelihood estimation restoration.

Spisula immunofluorescence and imaging

S. solidissima was obtained from the Marine Biological Laboratory (Woods Hole, MA), and zygotes were prepared as described (Palazzo and Vogel, 1999). Embryos were fixed with 4% formaldehyde/0.1% glutaraldehyde and stored at 4°C. A slurry of embryos was then treated with sodium borohydride (1 mg/ml) in phosphate-buffered saline (PBS) for 4 min (2×). Embryos were washed with PBS, permeabilized with PBS-Tween 20 (PBST), blocked with PBST plus 4% bovine serum albumin (BSA), and incubated overnight in either anti-tubulin (DM1alpha; Sigma-Aldrich, St. Lous, MO) or anti–γ-tubulin (T5192; Sigma-Aldrich) 1:200 in PBST plus 4% BSA all on a rotator at 4°C. Embryos were then washed in PBST (3×) and incubated in secondary antibody (Alexa Fluor 488; Life Technologies, Carlsbad, CA) at 1:1000 and 4′,6-diamidino-2-phenylindole (DAPI) at 1:200. Embryos were washed in PBS (3×), mounted in DABCO Mowiol, and sealed.

Quantification

C. elegans. All quantitative analysis was carried out with Ivision software (BioVision Technologies, Exton, PA). Anaphase rates of

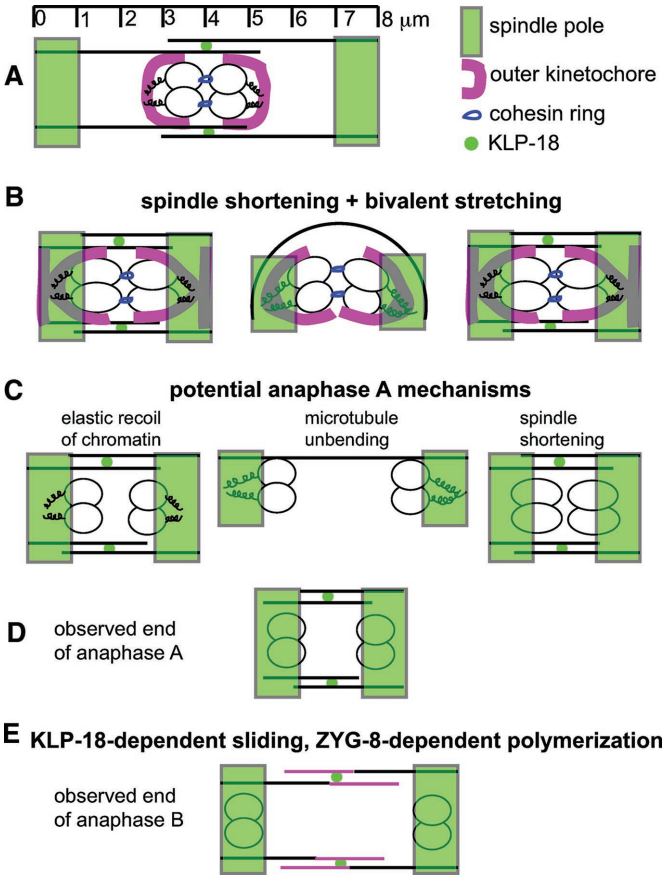

FIGURE 10: Model of *C. elegans* female meiotic anaphase I drawn to scale, showing a single bivalent within a single microtubule-poor channel. (A) Before APC activation, bivalents are oriented within the microtubule-poor channels of an 8-μm-long spindle in a KNL-1–dependent manner. (B) APC-dependent spindle shortening and kinetochore stretching result in a 4-μm-long spindle with the outer kinetochore overlapping the ASPM-labeled poles. (C) The predicted structures at the end of anaphase A that would result from each of three different kinetochore-independent mechanisms: elastic recoil of stretched chromatin, unbending of interpolar microtubule bundles, and spindle shortening. Although spindle shortening does not move chromosomes apart, it increases the overlap between homologues and poles. (D) The observed structure at the end of anaphase A. (E) The observed structure at the end of anaphase B. Pink lines indicate ZYG-8–dependent new microtubule polymer.

chromosome separation shown in Figures 2, 6C, and 8D were determined from time-lapse images of live embryos that express GFP::tubulin and mCherry::histone. Images were captured at 10- or 15-s intervals; they were then opened in Ivision and magnified so that the size of a homologue or sister chromatid was approximately equal to the size of the cursor and the cursor could be easily centered over it. Distances in micrometers were measured between separating homologues or sister chromatids, and rates are expressed as distance over time in minutes. "Perceived distance between homologs" before their separation (Figures 3C and 4A) is a measurement of the area between lobes with pixel intensity <50% of the pixel intensity in the centers of the lobes. Calculations in Figure 4, C and D, were made by subtracting the distance between the centers of homologues from the distance between the edges of ZWL-1::GFP cups for each individual chromosome. For distances shown in Figure 5, C and D, measurements were made across the entire spindle and then divided in half to determine the distance from the spindle center. Kymographs in Figure 8C were generated using ImageJ software.

Spisula. Distance between chromosomes in anaphase I was measured between the centers of each chromosome mass and included the *z*-distance. Similarly, the pole-to-pole distance was measured between the centers of each aster. Because the chromosomes are not separated in metaphase, they were plotted as having a distance of 1 μm.

ACKNOWLEDGMENTS

We thank Bruce Bowerman and the *Caenorhabditis* Genetics Center, which is funded by the National Institutes of Health Office of Research Infrastructure Programs (P40 OD010440), for *Caenorhabditis elegans* strains. We also thank Dan Starr, JoAnne Engebrecht, and Richard McKenny for critical reading of the manuscript. This work was supported by National Institute of General Medical Sciences Grant 1R01GM-079421 (to F.J.M.) and National Institutes of Health Training Grant T32 GM007377 (to D.C.).

REFERENCES

Albertson DG, Thomson JN (1982). The kinetochores of *Caenorhabditis elegans*. Chromosoma 86, 409–428.

Albertson DG, Thomson JN (1993). Segregation of holocentric chromosomes at meiosis in the nematode, *Caenorhabditis elegans*. Chromosome Res 1, 15–26.

Brust-Mascher I, Sommi P, Cheerambathur DK, Scholey JM (2009). Kinesin-5-dependent poleward flux and spindle length control in *Drosophila* embryo mitosis. Mol Biol Cell 20, 1749–1762.

Carabatsos MJ, Combelles CM, Messinger SM, Albertini DF (2000). Sorting and reorganization of centrosomes during oocyte maturation in the mouse. Microsc Res Tech 49, 435–444.

Cheeseman IM, Chappie JS, Wilson-Kubalek EM, Desai A (2006). The conserved KMN network constitutes the core microtubule-binding site of the kinetochore. Cell 127, 983–997.

Cheung K, Senese S, Kuang J, Bui N, Ongpipattanakul C, Gholkar A, Cohn W, Capri J, Whitelegge JP, Torres JZ (2016). Proteomic analysis of the mammalian katanin family of microtubule-severing enzymes defines KATNBL1 as a regulator of mammalian katanin microtubule-severing. Mol Cell Proteomics, mcp.M115.056465.

Connolly AA, Osterberg V, Christensen S, Price M, Lu C, Chicas-Cruz K, Lockery S, Mains PE, Bowerman B (2014). *Caenorhabditis elegans* oocyte meiotic spindle pole assembly requires microtubule severing and the calponin homology domain protein ASPM-1. Mol Biol Cell 25, 1298–1311.

Crowder ME, Flynn JR, McNally KP, Cortes DB, Price KL, Kuehnert PA, Panzica MT, Andaya A, Leary JA, McNally FJ (2015). Dynactin-dependent cortical dynein and spherical spindle shape correlate temporally with meiotic spindle rotation in *Caenorhabditis elegans*. Mol Biol Cell 26, 3030–3046.

Desai A, Rybina S, Müller-Reichert T, Shevchenko A, Shevchenko A, Hyman A, Oegema K (2003). KNL-1 directs assembly of the microtubule-binding interface of the kinetochore in *C. elegans*. Genes Dev 17, 2421–2435.

Drechsler H, McAinsh AD (2016). Kinesin-12 motors cooperate to suppress microtubule catastrophes and drive the formation of parallel microtubule bundles. Proc Natl Acad Sci USA 113, E1635–E1644.

Dumont J, Oegema K, Desai A (2010). A kinetochore-independent mechanism drives anaphase chromosome separation during acentrosomal meiosis. Nat Cell Biol 12, 894–901.

Ellefson ML, McNally FJ (2011). CDK-1 inhibits meiotic spindle shortening and dynein-dependent spindle rotation in *C. elegans*. J Cell Biol 193, 1229–1244.

Gassmann R, Essex A, Hu JS, Maddox PS, Motegi F, Sugimoto A, O'Rourke SM, Bowerman B, McLeod I, Yates JR 3rd, Oegema K, Cheeseman IM, Desai A (2008). A new mechanism controlling kinetochore-microtubule interactions revealed by comparison of two dynein-targeting components: SPDL-1 and the Rod/Zwilch/Zw10 complex. Genes Dev 22, 2385–2399.

Gönczy P, Bellanger JM, Kirkham M, Pozniakowski A, Baumer K, Phillips JB, Hyman AA (2001). *zyg-8*, a gene required for spindle positioning in *C. elegans*, encodes a doublecortin-related kinase that promotes microtubule assembly. Dev Cell 1, 363–375.

Griffis ER, Stuurman N, Vale RD (2007). Spindly, a novel protein essential for silencing the spindle assembly checkpoint, recruits dynein to the kinetochore. J Cell Biol 177, 1005–1015.

Gueth-Hallonet C, Antony C, Aghion J, Santa-Maria A, LajoieMazenc I, Wright M, Maro B (1993). gamma-Tubulin is present in acentriolar MTOCs during early mouse development. J Cell Sci 105, 157–166.

Hamill DR, Severson AF, Carter JC, Bowerman B (2002). Centrosome maturation and mitotic spindle assembly in *C. elegans* require SPD-5, a protein with multiple coiled-coil domains. Dev Cell 3, 673–684.

Heckmann S, Jankowska M, Schubert V, Kumke K, Ma W, Houben A (2014). Alternative meiotic chromatid segregation in the holocentric plant Luzula elegans. Nat Commun 5, 4979.

Heck MM, Pereira A, Pesavento P, Yannoni Y, Spradling AC, Goldstein LS (1993). The kinesin-like protein KLP61F is essential for mitosis in *Drosophila*. J Cell Biol 123, 665–679.

Higgins J, Midgley C, Bergh AM, Bell SM, Askham JM, Roberts E, Binns RK, Sharif SM, Bennett C, Glover DM, *et al.* (2010). Human ASPM participates in spindle organisation, spindle orientation and cytokinesis. BMC Cell Biol 11, 85.

Howe M, McDonald KL, Albertson DG, Meyer BJ (2001). HIM-10 is required for kinetochore structure and function on *Caenorhabditis elegans* holocentric chromosomes. J Cell Biol 153, 1227–1238.

Inoué S, Ritter H (1978). Mitosis in Barbulanympha. II. Dynamics of a two-stage anaphase, nuclear morphogenesis, and cytokinesis. J Cell Biol 77, 655–684.

Ito A, Goshima G (2015). Microcephaly protein Asp focuses the minus ends of spindle microtubules at the pole and within the spindle. J Cell Biol 211, 999–1009.

Kamath RS, Martinez-Campos M, Zipperlen P, Fraser AG, Ahringer J (2001). Effectiveness of specific RNA-mediated interference through ingested double-stranded RNA in *Caenorhabditis elegans*. Genome Biol 2, RESEARCH0002.

Kapitein LC, Peterman EJG, Kwok BH, Kim JH, Kapoor TM, Tarun M, Schmidt CF (2005). The bipolar mitotic kinesin Eg5 moves on both microtubules that it crosslinks. Nature 435, 114–118.

Kemp CA, Kopish KR, Zipperlen P, Ahringer J, O'Connell KF (2004). Centrosome maturation and duplication in *C. elegans* require the coiled-coil protein SPD-2. Dev Cell 6, 511–523.

Kikumoto M, Kurachi M, Tosa V, Tashiro H (2006). Flexural rigidity of individual microtubules measured by a buckling force with optical traps. Biophys J 90, 1687–1696.

Kirby C, Kusch M, Kemphues K (1990). Mutations in the par genes of Caenorhabditis elegans affect cytoplasmic reorganization during the first cell cycle. Dev Biol 142, 203–215.

Laan L, Pavin N, Husson J, Romet-Lemonne G, van Duijn M, López MP, Vale RD, Jülicher F, Reck-Peterson SL, Dogterom M (2012). Cortical dynein controls microtubule dynamics to generate pulling forces that position microtubule asters. Cell 148, 502–514.

Lydersen BK, Pettijohn DE (1980). Human-specific nuclear protein that associates with the polar region of the mitotic apparatus: distribution in a human/hamster hybrid cell. Cell 22, 489–499.

Maia AF, Tanenbaum ME, Galli M, Lelieveld D, Egan DA, Gassmann R, Sunkel CE, van den Heuvel S, Medema RH (2015). Genome-wide RNAi screen for synthetic lethal interactions with the *C. elegans* kinesin-5 homolog BMK-1. Sci Data 2, 150020.

Mallik R, Carter BC, Lex SA, King SJ, Gross SP (2004). Cytoplasmic dynein functions as a gear in response to load. Nature 427, 649–652.

McCarter J, Bartlett B, Dang T, Schedl T (1999). On the control of oocyte meiotic maturation and ovulation in *Caenorhabditis elegans*. Dev Biol 205, 111–128.

McNally FJ, Thomas S (1998). Katanin is responsible for the M-phase microtubule-severing activity in Xenopus eggs. Mol Biol Cell 9, 1847–1861.

McNally K, Audhya A, Oegema K, McNally FJ (2006). Katanin controls mitotic and meiotic spindle length. J Cell Biol 175, 881–891.

McNally K, Berg E, Cortes DB, Hernandez V, Mains PE, McNally FJ (2014). Katanin maintains meiotic metaphase chromosome alignment and spindle structure in vivo and has multiple effects on microtubules in vitro. Mol Biol Cell 25, 1037–1049.

McNally KL, Fabritius AS, Ellefson ML, Flynn JR, Milan JA, McNally FJ (2012). Kinesin-1 prevents capture of the oocyte meiotic spindle by the sperm aster. Dev Cell 22, 788–798.

McNally KP, McNally FJ (2011). The spindle assembly function of *Caenorhabditis elegans* katanin does not require microtubule-severing activity [correction published in Mol Biol Cell (2012). 23, 4472]. Mol Biol Cell 22, 1550–1560.

Monen J, Maddox PS, Hyndman F, Oegema K, Desai A (2005). Differential role of CENP-A in the segregation of holocentric *C. elegans* chromosomes during meiosis and mitosis [correction published in Nat Cell Biol (2006). 8, 100]. Nat Cell Biol 7, 1248–1255.

Moore LL, Morrison M, Roth MB (1999). HCP-1, a protein involved in chromosome segregation, is localized to the centromere of mitotic chromosomes in *Caenorhabditis elegans*. J Cell Biol 147, 471–480.

Mountain V, Simerly C, Howard L, Ando A, Schatten G, Compton DA (1999). The kinesin-related protein, HSET, opposes the activity of Eg5 and cross-links microtubules in the mammalian mitotic spindle. J Cell Biol 147, 351–366.

Muscat CC, Torre-Santiago KM, Tran MV, Powers JA, Wignall SM (2015). Kinetochore-independent chromosome segregation driven by lateral microtubule bundles. Elife 4, e06462.

Nasmyth K (2002). Segregating sister genomes: the molecular biology of chromosome separation. Science 297, 559–565.

Oegema K, Desai A, Rybina S, Kirkham M, Hyman AA (2001). Functional analysis of kinetochore assembly in *Caenorhabditis elegans*. J Cell Biol 153, 1209–1226.

O'Toole ET, McDonald KL, Mäntler J, McIntosh JR, Hyman AA, Müller-Reichert T (2003). Morphologically distinct microtubule ends in the mitotic centrosome of *Caenorhabditis elegans*. J Cell Biol 163, 451–456.

Palazzo RE, Vogel JM (1999). Isolation of centrosomes from *Spisula solidissima* oocytes. Methods Cell Biol 61, 35–56.

Paliulis LV, Nicklas RB (2004). Micromanipulation of chromosomes reveals that cohesion release during cell division is gradual and does not require tension. Curr Biol 14, 2124–2129.

Powers AF, Franck AD, Gestaut DR, Cooper J, Gracyzk B, Wei RR, Wordeman L, Davis TN, Asbury CL (2009). The Ndc80 kinetochore complex forms load-bearing attachments to dynamic microtubule tips via biased diffusion. Cell 136, 865–875.

Raaijmakers JA, Tanenbaum ME, Medema RH (2013). Systematic dissection of dynein regulators in mitosis. J Cell Biol 201, 201–215.

Rath U, Sharp DJ (2011). The molecular basis of anaphase A in animal cells. Chromosome Res 19, 423–432.

Ris H (1943). A quantitative study of anaphase movement in the aphid Tamalia. Biol Bull 85, 164–178.

Ris H (1949). The anaphase movement of chromosomes in the spermatocytes of the grasshopper. Biol Bull 96, 90–106.

Salje J, Gayathri P, Löwe J (2010). The ParMRC system: molecular mechanisms of plasmid segregation by actin-like filaments. Nat Rev Microbiol 8, 683–692.

Saunders W, Lengyel V, Hoyt MA (1997). Mitotic spindle function in *Saccharomyces cerevisiae* requires a balance between different types of kinesin-related motors. Mol Biol Cell 8, 1025–1033.

Saunders AM, Powers J, Strome S, Saxton WM (2007). Kinesin-5 acts as a brake in anaphase spindle elongation. Curr Biol 17, R453–R454.

Scholey JE, Nithianantham S, Scholey JM, Al-Bassam J (2014). Structural basis for the assembly of the mitotic motor Kinesin-5 into bipolar tetramers. Elife 3, e02217.

Sharp DJ, Yu KR, Sisson JC, Sullivan W, Scholey JM (1999). Antagonistic microtubule-sliding motors position mitotic centrosomes in *Drosophila* early embryos. Nat Cell Biol 1, 51–54.

Srayko M, Buster DW, Bazirgan OA, McNally FJ, Mains PE (2000). MEI-1/MEI-2 katanin-like microtubule severing activity is required for *Caenorhabditis elegans* meiosis. Genes Dev 14, 1072–1084.

Srayko M, Kaya A, Stamford J, Hyman AA (2005). Identification and characterization of factors required for microtubule growth and nucleation in the early *C. elegans* embryo. Dev Cell 9, 223–236.

Starr DA, Williams BC, Hays TS, Goldberg ML (1998). ZW10 helps recruit dynactin and dynein to the kinetochore. J Cell Biol 142, 763–774.

Straight AF, Sedat JW, Murray AW (1998). Time-lapse microscopy reveals unique roles for kinesins during anaphase in budding yeast. J Cell Biol 143, 687–694.

Tanenbaum ME, Macůrek L, Janssen A, Geers EF, Alvarez-Fernández M, Medema RH (2009). Kif15 cooperates with eg5 to promote bipolar spindle assembly. Curr Biol 19, 1703–1711.

Tao L, Mogilner A, Civelekoglu-Scholey G, Wollman R, Evans J, Stahlberg H, Scholey JM (2006). A homotetrameric kinesin-5, KLP61F, bundles

microtubules and antagonizes Ncd in motility assays. Curr Biol 16, 2293–2302.
Timmons L, Court DL, Fire A (2001). Ingestion of bacterially expressed dsRNAs can produce specific and potent genetic interference in *Caenorhabditis elegans*. Gene 263, 103–112.
van der Voet M, Berends CW, Perreault A, Nguyen-Ngoc T, Gönczy P, Vidal M, Boxem M, van den Heuvel S (2009). NuMA-related LIN-5, ASPM-1, calmodulin and dynein promote meiotic spindle rotation independently of cortical LIN-5/GPR/Galpha. Nat Cell Biol 11, 269–277.
Wignall SM, Villeneuve AM (2009). Lateral microtubule bundles promote chromosome alignment during acentrosomal oocyte meiosis. Nat Cell Biol 11, 839–844.
Yang HY, Mains PE, McNally FJ (2005). Kinesin-1 mediates translocation of the meiotic spindle to the oocyte cortex through KCA-1, a novel cargo adapter. J Cell Biol 169, 447–457.
Yang HY, McNally K, McNally FJ (2003). MEI-1/katanin is required for translocation of the meiosis I spindle to the oocyte cortex in *C. elegans*. Dev Biol 260, 245–259.